Draft version February 3, 2022
Preprint typeset using LaTeX style emulateapj v. 08/22/09

arXiv:0902.0373v1 [astro-ph.CO] 2 Feb 2009

THE ROLE OF DRY MERGERS FOR THE FORMATION AND EVOLUTION OF BRIGHTEST CLUSTER GALAXIES

M. Ruszkowski[1,2] and V. Springel[2]

Draft version February 3, 2022

ABSTRACT

Using a resimulation technique, we perform high-resolution cosmological simulations of dry mergers in a massive ($10^{15} M_{\odot}$) galaxy cluster identified in the *Millennium Run*. Our initial conditions include well resolved compound galaxy models consisting of dark matter halos and stellar bulges that are used to replace the most massive cluster progenitor halos at redshift $z = 3$, allowing us to follow the subsequent dry merger processes that build up the cluster galaxies in a self-consistent cosmological setting. By construction, our galaxy models obey the stellar mass-size relation initially. Also, we study both galaxy models with adiabatically contracted and uncompressed halos. We demonstrate that the brightest cluster galaxy (BCG) evolves away from the Kormendy relation as defined by the smaller mass galaxies (i.e., the relation *bends*). This is accompanied by a significantly faster dark matter mass growth within the half-light radius of the BCG compared to the increase in the stellar mass inside the same radius. As a result of the comparatively large number of mergers the BCG experiences, its total mass-to-light ratio becomes significantly higher than in typical elliptical galaxies. We also show that the mixing processes between dark matter and stars lead to a small but numerically robust tilt in the fundamental plane and that the BCG lies on the tilted plane. Our model is consistent with the observed steepening of the logarithmic mass-to-light gradient as a function of the stellar mass. As we have not included effects from gas dynamics or star formation, these trends are exclusively due to N-body and stellar-dynamical effects. Surprisingly, we find only tentative weak distortion in the Faber-Jackson relation that depends on the aperture size, unlike expected based on studies of isolated merger simulations. This may be due to differences in the distribution of galaxy orbits, which is given in our approach directly by the cosmological context while it has to be assumed in isolated merger simulations, and the fact that the BCG is located deep in the cluster potential well. Another uncertainty in both approaches lies in the definition of the spatial extent of the BCG.

Subject headings: clusters: general – galaxies: elliptical

1. INTRODUCTION

1.1. *What makes BCGs special ?*

The brightest cluster galaxies (BCGs) are special. They are the most massive and luminous galaxies in the Universe. They are typically located in the very centers of clusters of galaxies which indicates that their formation is closely linked to that of the clusters themselves. Their formation history is therefore distinct from typical elliptical galaxies (e.g., Lin & Mohr 2004, Brough et al. 2005, De Lucia & Blaizot 2006 and references therein). Recent analysis by Best et al. (2007) shows that BCGs are also more likely to host active galactic nuclei than other galaxies of the same stellar mass. This indicates that these objects play a pivotal role in quenching cooling flows and star formation in clusters.

BCGs have been recently shown to lie off the standard scaling relations of early-type galaxies (Lauer et al. 2007, von der Linden et al. 2007, Bernardi et al. 2007). In particular, they show excess luminosity (or stellar mass) above the prediction of the standard Faber-Jackson relation at high galaxy masses. This hints at the interesting possibility that their black hole masses may be larger than estimated from the $M - \sigma$ relation (Tremaine et al. 2002).

[1] Department of Astronomy, The University of Michigan, 500 Church Street, Ann Arbor, MI 48109, USA;
E-mail: mateuszr@umich.edu
[2] Max Planck Institute for Astrophysics, Karl-Schwarzschild-Str. 1, 85741 Garching, Germany;
E-mail: volker@map-garching.mpg.de

1.2. *Formation of BCGs in the cosmological context*

Early theoretical studies suggested that BCGs are formed as a result of star formation in *cooling flows* (Fabian 1994). However, recent X-ray observations performed with *Chandra* and *XMM Newton* show that cooling rates in nearby clusters are too low to explain the masses of BCGs. Tidal stripping and dynamical friction acting on the cluster galaxies have been suggested as an alternative BCG formation mechanism (Oemler 1976, Richstone 1976) but this mechanism turns out to be too slow due to the low cross section for galaxy-galaxy interactions in virialized cluster centers where relative velocities of galaxies are large (Ostriker 1980). Nevertheless, this *cannibalism* may be responsible for the formation of diffuse stellar envelopes extending up to hundreds of kiloparsecs (the 'cD' galaxies).

However, in a hierarchical structure formation theory, groups of galaxies will form before the formation and virialization of a cluster. Such groups have sufficiently small velocity dispersions that a significant number of galaxy-galaxy mergers occurs. This process should preferentially lead to the formation of elliptical galaxies in high galaxy density environments. Stellar population synthesis models demonstrate that the bulk of star formation in most massive galaxies took place prior to $z \sim 2$ (Thomas et

al. 2005, Treu et al. 2005, Jimenez et al. 2006). Semi-analytical models also show that stars that make up most of the BCG mass are formed very early on (80% by $z \sim 3$; De Lucia et al. 2006, De Lucia & Blaizot 2007). Only after most stars have been formed does the final galaxy assembly take place (the *downsizing* phenomenon; Bundy et al. 2005, Pannella et al. 2006, Calura et al. 2008, but see the revised monolithic collapse model of Chiosi & Carraro (2002) and the results of Cimatti et al. 2006 who, based on the same COMBO-17 and DEEP2 data as Bell et al. 2004, argue for "top-down" assembly of early-type galaxies, i.e., that downsizing concept may have to be extended to the mass assembly itself as the build-up of the most massive galaxies precedes that of the less massive ones.). Therefore, the final galaxy mergers in cluster formation are expected to be predominantly dissipationless (or *dry*, i.e. not involving large amounts of gas; Khochfar & Burkert 2003). This picture is also consistent with the analysis based on COMBO-17 results of Bell et al. (2004) who show that the stellar mass on the red sequence increased passively by a factor of ~ 2 since $z \sim 1$. We note that recent theoretical results suggest that the amount of gas associated with major mergers in the early Universe was much larger then at the present epoch (Khochfar & Silk 2006). Such *wet* mergers led to massive starbursts early on. However, at lower redshifts the amount of gas was much lower and the dominant mechanism for the galaxy growth in mass and size were dry mergers (e.g., Hopkins et al. 2008). This is evidenced indirectly by the strong size evolution of the most massive galaxies since $z = 2$ (Trujillo et al. 2007) while preserving the mass-size relation found by Trujillo et al. (2004).

Despite these findings, we note that the detailed picture of the giant elliptical assembly is further constrained by photometric and chemical observables. They suggest that it is difficult to explain giant elliptical by a pure sequence of multiple minor dry mergers or via major dry mergers (i.e., some admixture of wet mergers may be required to properly model chemical observables; Pipino & Matteucci 2008). However, the scatter in σ–[Mg/Fe] relation is large enough to permit one to three major dry mergers during the galactic lifetime (Bell et al. 2006). While the majority of BCGs from the sample studied by Bildfell et al. (2008) have bluer colors with increasing radius, about 25% possess bluer cores. The existence of such cores indicates that some cold gas must have been replenished in that subsample of BCGs at late epochs via minor wet mergers. Interestingly, Bildfell et al. (2008) find that the Kormendy relation of the BCGs is steeper than that of the local ellipticals. Kaviraj et al. (2008) argue that bright early-types potentially form 10-15 per cent of their stellar mass since z = 1 and, according to Pipino et al. (2008), the recent star formation in the blue core BCGs typically has an age less than 0.5 Gyrs and contributes mass fractions of less than a percent. von der Linden et al. (2007) show that BCGs exhibit higher [α/Fe] values than same mass ellipticals and claim that this indicated that star formation may have occurred over a shorter timescale in BCGs. This then suggests a possibility that the [α/Fe] radial gradients in BCGs could be consistent with being comparable to those in same mass ellipticals (Brough et al. 2005) rather then being unable to survive repeated dry mergers.

We also point out that the AGN feedback plays an important role in explaining the early and rapid formation of most massive ellipticals by shutting off star formation. The effect of AGNs may be felt more strongly in more massive galaxies that have been heated by virial shocks. This made their gas more dilute and more vulnerable to AGN feedback leading to passive evolution and 'red-and-dead' massive spheroids (Dekel & Birnboim 2006). Recent high-resolution *FLASH* code simulations of the interaction of relativistic jets with the ISM confirm that the star formation rate will be inhibited although it can increase on short time-scales of the order of $10^5 - 10^6$ yr Antonuccio-Delogu & Silk 2008).

As mentioned above, recent analysis of the *SDSS* and *Hubble* data demonstrates that BCGs form a separate class of objects that depart from the usual Faber-Jackson relation. This effect has been seen in numerical simulations of dry mergers performed by Boylan-Kolchin et al. (2006) who studied collisions of isolated galaxy pairs. They demonstrated that the initial orbital parameters play an important role in shaping the Faber-Jackson relation. In their model, galaxies that collide on more radial orbits, such as those present during the cluster assembly, lead to more puffed up merger remnants. Such final merger products are characterized by lower internal velocity dispersions than those resulting from lower ellipticity collisions. This mechanism is consistent with the fact that most massive galaxies experienced at least one merger since $z < 1.5$ (Conselice et al. 2007). As noted by Lauer et al. (2007), the increase in the ratio of the velocity dispersion of galaxies moving in the cluster potential to the internal velocity dispersion of individual cluster galaxies may also contribute to the puffing up effect. This is because some of the orbital energy of the colliding galaxies will be transferred to the internal energy of the merger remnant. Another effect that may influence the slope of the Faber-Jackson effect is tidal heating of galaxies moving in the cluster potential. It is due to all of the above complexities that one has to resort to cosmological simulations involving both the dark matter and stellar components to capture all relevant processes leading to the formation of BCGs. It is the purpose of this paper to address some of the above issues. We will deliberately use purely collisionless simulations, allowing us to obtain reliable N-body results in a fully cosmological context without having to delve into the complexities of gas dynamics and star formation. However, we note that the approach we outline here can be used also in future hydrodynamic simulations of the cluster formation process.

The paper is organized as follows. In Section 2, we outline the numerical approach used to simulate the cluster and its galaxies. Section 3 discusses our results (scaling relations, tilt in the fundamental plane, the evolution of the mass-to-light ratio, and merger rates). Then in Section 4, we discuss the numerical convergence and the dependence of our results on the initial conditions and the galaxy models. Finally, Section 5 summarizes our findings.

2. METHODS

Our approach to simulate the evolution of the BCG is similar in spirit to that of Dubinski (1998), who replaced 100 dark halos at $z = 2$ in a proto-cluster region

with galaxy models constructed in isolation, and then continued the simulation to the present epoch. However our method differs in several important details, and for definiteness, we list its primary steps in the following:

- We identify a massive $10^{15} M_\odot$ cluster at $z = 0$ in the *Millennium Run* (Springel et al. 2005a) and track its particles back to the initial conditions.
- We determine the Lagrangian region of the cluster material in the original unperturbed initial conditions and produce a new refined unperturbed particle load at $z = 127$ which is adequate for a *zoom simulation* onto the selected target halo at higher resolution.
- We generate the actual initial conditions by perturbing the particle load obtained in the previous point with the Millennium displacement field, augmented with additional small-scale waves that can now be added due to the improved mass resolution of $\simeq 10^9 h^{-1} M_\odot / F_{\rm zoom}^3$. We consider $F_{\rm zoom} = 2$ and $F_{\rm zoom} = 4$ in this paper, corresponding to approximately 8 and 64 times the original resolution. Further away from the cluster, the resolution is progressively downgraded in mass, and the gravitational softening lengths are enlarged, ensuring however that the tidal forces acting on the high-resolution region are represented accurately at all times.
- We evolve these initial conditions to $z = 3.0$.
- We identify the fifty most massive dark matter halos at this redshift (almost all of them end up in the final cluster) and replace them with galaxy models at either the same mass resolution as in the high-resolution region, or with the resolution enhanced by another factor of eight. The models consist of both dark matter and stellar particles (see below). In every run the dark matter and star particles of galaxy models have the same mass in order to minimize differential two-body heating effects between the two components. The maximum mass and force resolutions for each of our simulations are listed in Section 3.
- We evolve the cluster from $z = 3.0$ to the present epoch.

We note that this approach is also similar in spirit to that recently employed by Rudick, Mihos & McBride (2006) who focused on the problem of the intracluster light and studied significantly less massive ($\sim 10^{14} M_\odot$) clusters. We only consider spheroidal galaxy models in this paper that include a stellar bulge and a dark matter halo. The bulge size obeys the size-stellar mass relation of Shen et al. (2003):

$$R_e = 4.16 h^{-1} \left(\frac{M_{\rm star}}{10^{11} h^{-1} M_\odot} \right)^{0.56} {\rm kpc}, \qquad (1)$$

where R_e is the half-light radius, and $M_{\rm star}$ is the stellar mass of a given galaxy. There is observational evidence (Trujillo et al. 2004, McIntosh et al. 2005) that this relation remains unchanged up to $z \sim 1$ as long as the most massive ellipticals are excluded. Note that more recent observations suggest that the size-luminosity relation evolves with redshift for high-mass ellipticals (Zirm et al. 2007, van Dokkum et al. 2008) but at these mass scales this trend is naturally explained by our simulations as explained in section 3). For the sake of simplicity we here assume that the relation also holds at our redshift ($z = 3$) for constructing the initial galaxy models (see Section 3 for more discussion of this assumption). We describe the distribution of mass in stars $m_*(r)$ in the bulge by a Hernquist profile, i.e.,

$$\rho_*(r) = \frac{M_*}{2\pi} \frac{a}{r(r+a)^3}, \qquad (2)$$

where a is a characteristic radius, M_* is the total mass of the stellar component in a given galaxy and r is the distance from its center. We truncate the Hernquist profile at $r = 10\,a$ in our numerical realizations in order to avoid the occurrence of a very small number of very distant star particles. For this choice of parameters, the half-light radius is $R_e = 1.339\,a$.

We assume that 90% of the original dark matter mass of each halo excised from the zoomed Millennium simulation consists of dark matter and the rest contributes to the stellar component. The dark matter halos are modeled with the NFW profile (Navarro, Frenk & White 1996) truncated at r_{200}, with a concentration parameter $c_{\rm vir}$ given by a modified version of the Bullock et al. (2001) prescription,

$$c_{\rm vir}(\mu, a) = K \frac{a}{a_c}, \qquad (3)$$

where K is a constant, $a = 1/(1+z)$, $a_{\rm c}$ is the epoch of collapse of a given halo and $\mu = M_{\rm vir}(a)/M_*(a)$ is a ratio of a halo mass and the typical halo mass at the same epoch a. The typical mass at an epoch a is defined as $\sigma[M_*(a)] = 1.686/D(a)$, where $D(a)$ is the linear growth factor and $\sigma(M)$ is the rms density fluctuation on a comoving scale containing the mass M. The collapse epoch is defined by $M_*(a_c) = F M_{\rm vir}$, where F is a free parameter. In the computation of $c(\mu, a)_{\rm vir}$, as well as in all of our simulation runs (carried out with the GADGET-3 code; Springel 2005c), we assume the cosmological parameters of the Millennium Run, given by $\Omega_{\rm m} = 0.25$, $\Omega_\Lambda = 0.75$, a scale invariant slope of the power spectrum of primordial fluctuations ($n = 1.0$), a fluctuation normalization $\sigma_8 = 0.9$, and a Hubble constant of $H_0 = 100\,h\,{\rm km\,s^{-1}\,Mpc^{-1}} = 73\,{\rm km\,s^{-1}\,Mpc^{-1}}$. The constants $K = 3.4$ and $F = 0.01$ have been chosen following Macciò et al. (2006). We note that recently Gao et al. (2008) have provided a yet more accurate parametrization of the concentration dependence on mass and redshift than given by equation (3), but our results are insensitive to the size of this revision.

Once the density structure of our galaxy models has been specified, velocity distributions of the bulge and dark matter particles are obtained by solving the Jeans equations following the method of Springel et al. (2005b). For the sake of simplicity, we assume that the dark matter halos have zero net angular momentum.

Where indicated, the dark matter distribution has been modified by including adiabatic contraction follow-

ing the classic Blumenthal et al. (1986) approximation. Hydrodynamical simulations by Gnedin et al. (2004) suggest that this approximation overpredicts the amount of contraction at small radii. We note however that these differences between hydrodynamical simulations and the contraction model are smaller than the differences between the uncompressed and contracted halos, and that an overestimate of the contraction effect allows us to *bracket* reality between the two models we consider.

Nevertheless, we want to stress that our toy galaxy models are too simplistic to represent real galaxies very accurately. However, the advantage of our approach is that it gives us better control over the parameters of the galaxy population under study and allows us to cleanly separate the pure N-body effects from the complicated physics of gas dynamics, radiative cooling, star formation, etc. Our method should still be sufficiently accurate to investigate the evolution of the main trends in galaxy scaling relation, especially in the K-band. While the luminosity of the early type galaxies on the red sequence does evolve with redshift, the passive stellar evolution does not change the K-band luminosity much and hence should not dramatically affect our results. This approach differs from, e.g., that of Conroy et al. (2006) and Berrier et al. (2008) who combine dark matter simulations with recipes for assigning light to dark matter halos and study the assembly of a large number of clusters, or from that of Murante et al. (2007) who incorporate the gasdynamical effect and star formation at the expense of lower dynamical range.

In our analysis, the BCG was identified using first the friends-of-friends algorithm to find the cluster halo and its galaxies, and then by applying the SUBFIND group finding algorithms to look for gravitationally bound structures. We did not set any strict isophotal limit when defining galaxies, instead we let SUBFIND identify the bound stellar and dark matter part. This sets a certain isophotal limit for the BCG. The corresponding isophotal limit for non-BCGs may be slightly different but that should not affect their half-light radii significantly as they do not possess extended envelopes. Moreover, unless the change in the isophotal limits is huge, it is not likely to substantially affect the total luminosities and half-light radii of the galaxies in our sample.

3. RESULTS

All results presented in this section correspond to our default case where the initial galaxy models were adiabatically contracted. For details of the numerical parameters for all runs see Section 4. Figure 1 shows the evolution of the relation between the half-light radius R_e and the stellar mass within that radius. This relation is similar to the Kormendy relation. The initial ($z = 3$) and final ($z = 0$) models are represented by the red and black points, respectively. Intermediate redshifts are marked by open circles with colors as given in the inset. The figure demonstrates that, while smaller mass galaxies show relatively little evolution, the BCG clearly gains a substantial amount of mass and increases in size. Interestingly, it clearly evolves off the extrapolation of the initial radius-mass relation. We stress that, in the current scenario, this effect is entirely due to N-body process and is not caused by gas-dynamical processes, radiative cooling, star formation, etc. This effect has been reported in the observational work of Lauer et al. (2007). They showed that the half-light radii of BCGs lie above the log-log relation between the half-light radius and stellar luminosity defined by smaller mass galaxies. They also attribute this effect to a "progressive change in the character of 'dry mergers' at higher galaxy masses". This has also been reported even more recently by Bildfell et al. 2008 who state that "the Kormendy relation of our BCGs is steeper than that of the local ellipticals, suggesting differences in the assembly history of these types of systems." We also note that the trend for the size of the most massive galaxies to evolve with redshift (Zirm et al. 2007, van Dokkum et al. 2008) is consistent with the evolution of our simulated relation. Interestingly, our results also imply the steepening of the logarithmic mass-to-light gradient as a function of the stellar mass. The logarithmic M/L gradient (Napolitano et al. 2005) evaluated using $r_{\rm in} = R_{\rm e}$ and $r_{\rm out} = R_{\rm vir}$ is approximately $\nabla_l\gamma \approx (R_{\rm e}/R_{\rm vir})[(M_{\rm DM}/M_s)_{\rm out} - (M_{\rm DM}/M_s)_{\rm in}] \propto R_{\rm e}/R_{\rm vir}$ because $R_{\rm e} \ll R_{\rm vir}$, $(M_{\rm DM}/M_s)_{\rm out} \gg (M_{\rm DM}/M_s)_{\rm in}$ and $(M_{\rm DM}/M_s)_{\rm out}$ is a constant ($M_{\rm DM}$ and M_s denote the dark matter and stellar masses enclosed within a given radius, respectively). Since $R_{\rm e} \propto M_s^{\alpha}$, we have $\nabla_l\gamma \propto M_s^{\alpha-1/3}$. Now, for $\alpha = 0.56$ the relation is flat while for higher stellar masses α increases and so does the logarithmic M/L gradient. This is in agreement with the observational findings of Napolitano et al. (2005).

Figure 2 shows the evolution of the stellar (violet) and dark matter (red) components within the half-light radius of the BCG as a function of redshift. The values on the vertical axis are normalized to the dark matter mass within the half-light radius at $z = 3$. It is evident from this figure that the bend in the $R_e - M$ relation is accompanied by a significant gain in mass of the BCG both in terms of the stellar and dark matter components. Interestingly, the ratio of the dark matter-to-stellar mass increases with time significantly. In other words, the regions of the BCG within the half-light radius become disproportionally more massive with time for a given stellar luminosity. We note that the stellar mass accretion rates of BCGs (a factor of ~ 2.5 since $z \sim 2$) obtained by Romeo et al. (2008) are consistent with our findings.

The change in the dark matter-to-stellar mass ratio is likely caused by the large number of mergers that the BCG experiences over time, especially when compared to other galaxies. In Figure 3 we show a histogram of the number of mergers experienced by the BCG, the second largest and the third largest galaxy in the cluster. A merger is here defined as an event where over 50% of the stellar mass from one galaxy ends up in another galaxy. The vertical axis is for the cumulative number of mergers from the initial redshift $z_{\rm ini} = 3$ down to a given redshift $z < z_{\rm ini}$ (shown on the horizontal axis). As is clearly seen, the number of mergers declines rapidly with galaxy mass, and most of the mergers happening in the cluster are between the BCG and smaller galaxies.

We note that the results for the most massive galaxies are quite insensitive to the exact definition of the n-th most massive galaxy, which can be defined as either (i) n-th largest at a given redshift or (ii) n-th largest at $z = 0$. Strictly speaking, we adopt the latter definition and backtrace the history of the particles belonging to such-defined n-th largest galaxies in the computational

volume. The fact that the results for the most massive objects do not depend on the choice of the definition shows that the most massive galaxies preserve their identities and it is mostly smaller objects that accrete onto them. The Figure 3 indeed confirms that the BCG experiences overwhelmingly more mergers than smaller galaxies. This fact is the key reason for the change in the mass ratio between dark matter and the stellar component within the BCG's half-light radius. The number of mergers experienced by the most massive galaxy is zero between $z = 2$ and $z = 3$ and the smaller the galaxy mass the lower the redshift at which it experiences a merger (if any). Therefore, the results are not sensitive to the exact insertion redshift for the galaxy models.

We note that the boost in the dark matter to stellar mass ratio could be contaminated by mergers of small starless halos (which were not replaced with galaxy models) with a bigger halo. However, the dynamical friction time is a strongly decreasing function of the mass of the object that is merging with a bigger one. Therefore, the contribution to the growth in the BCG mass that comes from the small halos that we do not populate with stars is expected to be weak. This fact is not inconsistent with the above observation that the most massive objects do not merge with the BCG. It simply means that among the objects within a certain mean distance from each other, the most massive ones are the first ones to merge. In other words, the biggest galaxies in our simulations have simply been prevented from merging thus far by their large distance.

Curiously, the stellar mass-σ dispersion shown in Figure 4 does not show strong bend similar to that presented in Figure 1. Figure 4 shows the evolution of the stellar mass within the half-light radius and the velocity dispersion σ which, in our model, is essentially an equivalent of the Faber-Jackson relation. The initial slope of this relation is ~ 3.62. The meaning of the symbols is the same as in Figure 1. The stellar velocity dispersions are measured within half-light radii, are three-dimensional (i.e., all three components of velocity are used to compute them) and are intensity-weighted (i.e., in our case, weighted by the stellar mass integrated along the line-of-sight). At the final redshift the BCG lies on the relation defined by the extrapolation of the initial galaxy models to more massive objects.

The right panel shows the flux-weighted σ as a function of stellar mass for three different apertures: half-light radius (red points), 1/8 or the half-light radius (green points) and 1/16 of that radius (blue points). There is a systematic trend for the BCG to move to smaller velocity dispersions as the size of the aperture is decreased. At the same time, low-σ objects only increase their scatter around the unaltered mean values. There is also a tentative weak hint of a *bend* in this relation but this conclusion depends on the precise measurement of lowest σ galaxies that show scatter and the magnitude of the bend may be slightly affected by the precise definition of the BCG boundary that separates it from the intracluster light (ICL).

We also note that the dependence of sigma on luminosity is slightly more subtle. In the case of size-luminosity relation, for a given binding energy of the merging pair, the satellites on high angular orbits need to lose more angular momentum to merge and then end up being more compact. Those on lower angular momentum orbits are then more puffed up. On the other hand, the velocity dispersion close to the galactic center is strongly influenced by the stellar bulge and declines with radius up to a point where the cluster potential starts to dominate leading to the increase of the dispersion with the distance from the BCG center. This means that the cluster potential may try to slow down the increase of the slope with luminosity of the Faber-Jackson relation. In any case, fitting the extended wings of the BCG light distribution, beyond of the extent of this central galaxy as identified in our on-the-fly algorithm, could perhaps increase the bend in this relation (and the Kormendy relation) slightly and allow one to study the evolution of the ICL but such effects should not dramatically alter our conclusions. We defer such detailed analysis to a forthcoming publication.

Liu et al. (2008) analyzed a sample of BCGs and ellipticals and found that the slope of both the size-luminosity and the Faber-Jackson relation changes with the galaxy luminosity. However, they also analyzed BCGs and bright ellipticalls falling into the same magnitude range. Curiously, they found that, while "the power-law indices for the size-luminosity relations for BCGs are steeper then those for bright non-BCG elliptical galaxies, the power-law indices for the Faber-Jackson relations are also steeper, but only at $\sim 1\sigma$ levels, and so are not statistically significant" (see their Figure 14). This trend appears to be consistent with our simulations. The departure of the BCG from the original log-log size-luminosity relation increases with time and the slope of the size-luminosity for the BCG also seems to rise. This clearly suggests that an ensemble of simulated clusters would show a different size-luminosity slope for BCG and non-BCG galaxies in the same luminosity range, but a reliable determination of the size of the effect would require a much larger simulation set.

Finally, Figure 5 shows the "fundamental plane" corresponding to the initial models at $z = 3$ (red points) and the galaxies at the final redshift $z = 0$ (violet points). The "brightness" parameter is $I_e = m_{\rm stars}/(\pi R_e^2)$, where $m_{\rm stars}$ is the stellar mass within the half-light radius. The absolute values on the axes are not important here as we are only interested in the evolution of the slope of this relation. The initial slope of the relation is ~ 0.83 (by definition, the virial relation corresponds to 1.0). Indeed, there appears to be a small but numerically robust tilt in the fundamental plane. The final slope of the relation is ~ 0.72. The BCG seems to lie on the tilted plane but, strictly speaking, this conclusion depends on the robustness of the values measured for the least massive galaxies (see below for a discussion of numerical convergence). Nevertheless, the trend for the most massive object(s) to move away from the original relation is real. We stress again that this effect is entirely due to stellar dynamical/N-body effects.

4. NUMERICAL CONVERGENCE AND MODEL ROBUSTNESS

We performed several test runs in order to assess the numerical convergence of our results and their sensitivity to the initial galaxy models. For testing the basic numerical convergence we in general used uncontracted galaxy models; these have less particles inside the half-light radii and therefore yield more conservative convergence tests.

Figure 6 shows one of the results of these tests. It presents the relation between the half-light radius and the stellar mass within that radius. Initial models are denoted by open red circles. All other points are for the galaxies at the final redshift $z = 0$. Different sets of points grouped by color correspond to different resolutions. In this figure, we show the results for four different runs:

- run A: maximum mass resolution at the baseline level of the zoom simulation equal to $1.25 \times 10^8 h^{-1} M_\odot$, combined with a maximum force resolution of $2\,h^{-1}$kpc.
- run B: baseline mass resolution unchanged, but the mass resolution of the galaxy models enhanced further by a factor of eight.
- run C: same as above, but the gravitational softening length for the particles in the galaxy models was decreased by a factor of two.
- run D: baseline mass resolution enhanced further by a factor of eight to $1.50 \times 10^7 h^{-1} M_\odot$, mass resolution of the galaxy models equal to the baseline mass resolution, and a gravitational force resolution equal to $1\,h^{-1}$kpc everywhere in the high-resolution region.

The runs A to D show progressively improving agreement as the resolution of the simulations is increased. This is especially evident for the smallest objects. The comparison of the runs C and D shows that the effects of two-body relaxation do not play an important role even in the lower resolution run C. The maximum resolution run exhibits a close agreement of the galaxy properties at $z = 0$ with those assumed at the initial redshift. As in the case of Figure 1, this figure shows a clear bend in the Kormendy relation but this time for the galaxy models that were not adiabatically compressed.

In Figure 7, we show how the mass ratios evolve as a function of stellar mass. The color coding is the same as in Figure 1. The left panel is for the uncompressed initial models and the right one for the adiabatically contracted ones. As expected, the adiabatically contracted models have higher dark matter to stellar mass ratios. Nevertheless, the conclusions remain the same. The obvious trend for the BCG to evolve in a dramatically different fashion than the rest of the population in the cluster is present. The conclusion regarding all other plots discussed above also hold for the models that were not adiabatically compressed.

The mass of the cluster of galaxies considered here ($10^{15} M_\odot$) is much greater then the total mass in the entire computational volume ($\sim 4 \times 10^{13} M_\odot$) considered in the cosmological simulations of the fundamental plane and scaling relations presented by Oñorbe et al. (2006). Their simulations include the effects of gas cooling and star formation. However, the mass resolution in our case is much better than the resolution of 2×64^3 particles these authors considered. It is not clear if their results are numerically fully converged at $z = 0$ as their convergence tests were performed at $z = 1$ due to the very high CPU requirements. Oñorbe et al. (2006) do not report a departure of the most massive object from the scaling relations but they do see a tilt in the fundamental plane. In their model, the tilt is created during an early violent phase of rapid cooling and star formation. This tilted fundamental plane is then preserved in the dissipationless mergers that follow.

We acknowledge that we can afford the very high numerical resolution and dynamical range we achieve in our cluster only at the expense of not including gas dynamical effects but, as a result, this allows us to address a very clean and well-defined problem and to isolate the purely dynamical effects from the complicated gas dynamical processes. Also, in our approach we can ensure by construction that the galaxies at the initial high redshift obey a prescribed mass-size relation, which further helps to make the problem we examine clean and well defined, and to arrive at robust conclusions.

5. CONCLUSIONS AND DISCUSSION

We have performed high dynamical range cosmological N-body simulation of the formation of a massive $10^{15} M_\odot$ cluster of galaxies. We included both the stellar and dark matter particle components in order to investigate the (differential) evolution of these two components and the relationship between them. We also performed numerical convergence tests and checked the robustness of our approach with respect to details of the initial galaxy models by considering both regular and adiabatically compressed galaxy models.

In our approach, the Kormendy relation (defined here as the relation between the half-light radius and the mass in the stellar component) evolves with redshift entirely due to stellar dynamical/N-body processes. More specifically, the BCG clearly departs from the extrapolation of the initial relation to higher mass objects and the final relation appears to be bent at the massive end. The evolution of the BCG is accompanied by a systematic and strong increase in the dark matter-to-stellar mass ratio which is brought about by a significantly larger number of mergers that the BCG experiences compared with other galaxies. In contrast, smaller galaxies show rather little evolution in this proxy of the mass-to-light ratio. We speculate that the above trend also implies that the slope of the $R_e - L$ relation for the BCGs is steeper than for the smaller early-type galaxies. This possibility would have to be explored in future simulations involving more clusters of varying mass. Interestingly, a gentle trend for this quantity to increase with the galaxy mass has been reported by Gallazzi et al. (2006) in early-type galaxies in the SDSS survey. The bend in the Kormendy relation has also been interpreted by Lauer et al. (2007) as being due to an increase in this mass ratio. We note that such variations may also have important implications for the lensing properties of the BCGs.

Surprisingly, the Faber-Jackson relation only shows a tentative weak bending with redshift in our simulations that depends on the aperture size. However, isolated merger experiments performed mostly for parabolic merger orbits (Boylan-Kolchin et al. 2006) suggest that such an effect could be present. We speculate that the key factors responsible for this difference are: (1) the mergers in our model all take place in the central cluster potential and the BCG lies very close to it and (2) our initial conditions for the mergers are self-consistently taken into account as we evolve all galaxies in the cos-

mological context starting from high redshift prior to the cluster assembly. We also note that the distribution of the initial orbital parameters of the merging galaxies is a very sensitive function of eccentricity. More precisely, the distribution possesses a narrow spike at zero eccentricity (Benson 2005), and small departures from the idealized case of parabolic orbits are then likely in a realistic scenario, and (3) the precise definition of where the BCG envelope ends and the ICL component begins may somewhat modify the measured strength of any bend in these relations.

ACKNOWLEDGMENTS

MR acknowledges support from the *Chandra* theory grant TM8-9011X. MR thanks Anja von der Linden, Monica Valluri, Marta Volonteri, Mike Boylan-Kolchin, Massimo Dotti, Ole Möller, Eric Bell and Simon White for many stimulating discussions and Klaus Dolag for technical help in the early stages of this project. The runs were performed on the OPA cluster at the Rechenzentrum Garching of the Max-Planck-Society and on the *Columbia* supercomputer at NASA NAS Ames center. It is MR's pleasure to thank the staff of NAS, and especially Johnny Chang and Art Lazanoff, for their highly professional help. We thank the referee for a very constructive report that greatly helped to improve the paper.

REFERENCES

Antonuccio-Delogu, V., & Silk, J. 2008, MNRAS, 389, 1750
Bell, E. F., et al. 2004, ApJ, 608, 752
Bell, E. F., et al. 2006, ApJ, 640, 241
Benson, A. J. 2005, MNRAS, 358, 551
Bernardi, M., Hyde, J. B., Sheth, R. K., Miller, C. J., & Nichol, R. C. 2007, AJ, 133, 1741
Berrier, J. C., Stewart, K. R., Bullock, J. S., Purcell, C. W., Barton, E. J., & Wechsler, R. H. 2008, ArXiv e-prints, 804, arXiv:0804.0426
Best, P. N., von der Linden, A., Kauffmann, G., Heckman, T. M., & Kaiser, C. R. 2007, MNRAS, 379, 894
Bildfell, C., Hoekstra, H., Babul, A., & Mahdavi, A. 2008, MNRAS, 389, 1637
Blumenthal, G. R., Faber, S. M., Flores, R., & Primack, J. R. 1986, ApJ, 301, 27
Boylan-Kolchin, M., Ma, C.-P., & Quataert, E. 2006, MNRAS, 369, 1081
Brough, S., Collins, C. A., Burke, D. J., Lynam, P. D., & Mann, R. G. 2005, MNRAS, 364, 1354
Bullock, J. S., Kolatt, T. S., Sigad, Y., Somerville, R. S., Kravtsov, A. V., Klypin, A. A., Primack, J. R., & Dekel, A. 2001, MNRAS, 321, 559
Bundy, K., Ellis, R. S., & Conselice, C. J. 2005, ApJ, 625, 621
Calura, F., Jimenez, R., Panter, B., Matteucci, F., & Heavens, A. F. 2008, ApJ, 682, 252
Cimatti, A., Daddi, E., & Renzini, A. 2006, A&A, 453, L29
Chiosi, C., & Carraro, G. 2002, MNRAS, 335, 335
Conroy, C., Wechsler, R. H., & Kravtsov, A. V. 2007, ApJ, 668, 826
Conselice, C. J., et al. 2007, MNRAS, 381, 962
Dekel, A., & Birnboim, Y. 2006, MNRAS, 368, 2
De Lucia, G., Springel, V., White S. D. M., Croton D., Kauffmann G. 2006, MNRAS, 366, 499
De Lucia, G., & Blaizot, J. 2007, MNRAS, 375, 2
Dubinski, J. 1998, ApJ, 502, 141
Fabian, A. C. 1994, ARA&A, 32, 277
Gallazzi, A., Charlot, S., Brinchmann, J., & White, S. D. M. 2006, MNRAS, 370, 1106
Gao, L., Navarro, J. F., Cole, S., Frenk, C. S., White, S. D. M., Springel, V., Jenkins, A., & Neto, A. F. 2008, MNRAS, 387, 536
Gnedin, O. Y., Kravtsov, A. V., Klypin, A. A., & Nagai, D. 2004, ApJ, 616, 16
Hopkins, P. F., Hernquist, L., Cox, T. J., Keres, D., & Wuyts, S. 2008, arXiv:0807.2868
Kaviraj, S., et al. 2008, MNRAS, 388, 67
Khochfar, S., & Burkert, A. 2003, ApJ, 597, L117
Khochfar, S., & Silk, J. 2006, ApJ, 648, L21
Jimenez, R., Bernardi, M., Haiman, Z., Panter, B., & Heavens, A. F. 2007, ApJ, 669, 947
Lauer, T. R., et al. 2007, ApJ, 662, 808
Lin, Y.-T., & Mohr, J. J. 2004, ApJ, 617, 879
Liu, F. S., Xia, X. Y., Mao, S., Wu, H., & Deng, Z. G. 2008, MNRAS, 385, 23
Macciò, A. V., Dutton, A. A., van den Bosch, F. C., Moore, B., Potter, D., & Stadel, J. 2007, MNRAS, 378, 55
McIntosh, D. H., et al. 2005, ApJ, 632, 191
Murante, G., Giovalli, M., Gerhard, O., Arnaboldi, M., Borgani, S., & Dolag, K. 2007, MNRAS, 377, 2
Navarro, J. F., Frenk, C. S., & White, S. D. M. 1996, ApJ, 462, 563
Oemler, A., Jr. 1976, ApJ, 209, 693
Oñorbe, J., Domínguez-Tenreiro, R., Sáiz, A., Artal, H., & Serna, A. 2006, MNRAS, 373, 503
Ostriker, J. P. 1980, Comments on Astrophysics, 8, 177
Pannella, M., Hopp, U., Saglia, R. P., Bender, R., Drory, N., Salvato, M., Gabasch, A., & Feulner, G. 2006, ApJ, 639, L1
Pipino, A., & Matteucci, F. 2008, A&A, 486, 763
Pipino, A., Kaviraj, S., Bildfell, C., Hoekstra, H., Babul, A., & Silk, J. 2008, arXiv:0807.2760
Richstone, D. O. 1976, ApJ, 204, 642
Romeo, A. D., Napolitano, N. R., Covone, G., Sommer-Larsen, J., Antonuccio-Delogu, V., & Capaccioli, M. 2008, MNRAS, 389, 13
Rudick, C. S., Mihos, J. C., & McBride, C. 2006, ApJ, 648, 936
Shen, S., Mo, H. J., White, S. D. M., Blanton, M. R., Kauffmann, G., Voges, W., Brinkmann, J., & Csabai, I. 2003, MNRAS, 343, 978
Springel, V., et al., 2005a, Nature, 435, 629
Springel, V., Di Matteo, T., & Hernquist, L. 2005b, MNRAS, 361, 776
Springel, V. 2005c, MNRAS, 364, 1105
Thomas, D., Maraston, C., Bender, R., & Mendes de Oliveira, C. 2005, ApJ, 621, 673
Tremaine, S., et al. 2002, ApJ, 574, 740
Treu, T., et al. 2005, ApJ, 633, 174
Trujillo, I., et al. 2004, ApJ, 604, 521
Trujillo, I., Conselice, C. J., Bundy, K., Cooper, M. C., Eisenhardt, P., & Ellis, R. S. 2007, MNRAS, 382, 109
van Dokkum, P. G., et al. 2008, ApJ, 677, L5
von der Linden, A., Best, P. N., Kauffmann, G., & White, S. D. M. 2007, MNRAS, 379, 867
Zirm, A. W., et al. 2007, ApJ, 656, 66

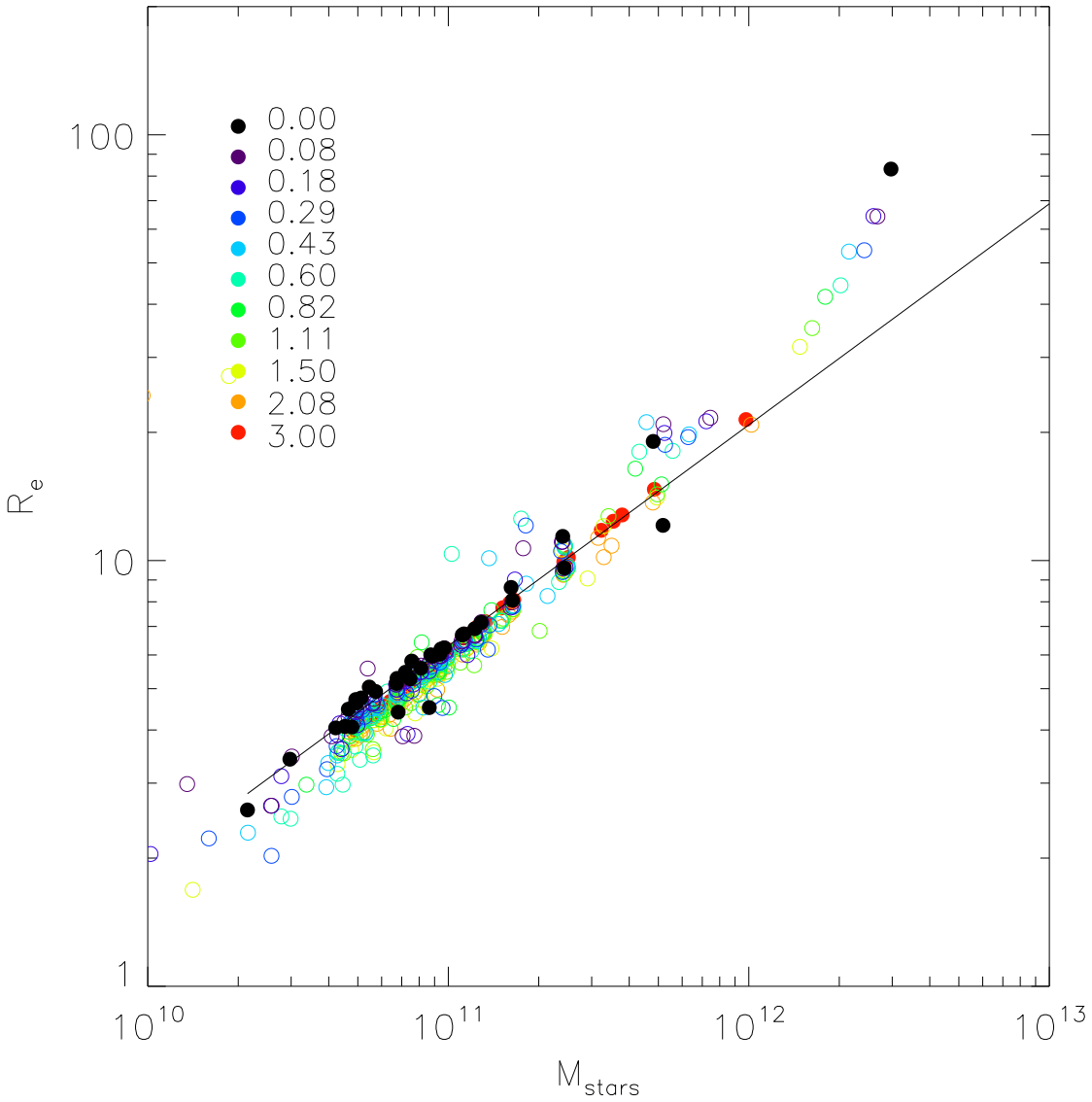


FIG. 1.— Half-light radius vs. stellar mass relation. Filled red circles are for the initial models at $z = 3$ and the black ones are for $z = 0$. Intermediate redshift data is shown as open circles and distributed in redshift according to the color scale given in the upper left corner.

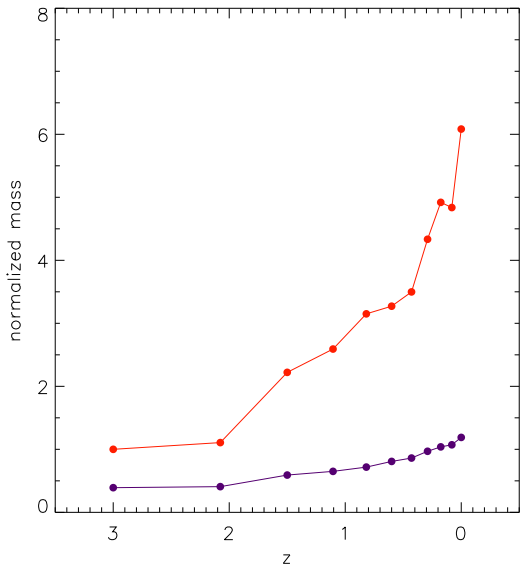


FIG. 2.— Mass in the dark matter (red) and stellar (violet) components for the BCG as a function of redshift. The values are normalized to the dark matter mass within the half-light radius at $z = 3$.

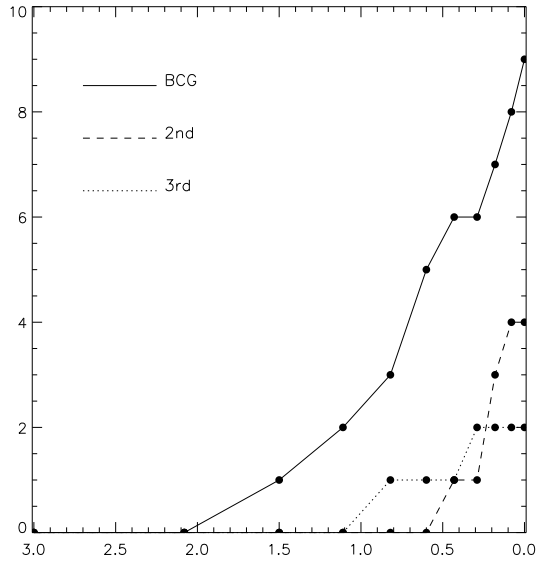


FIG. 3.— Cumulative number of mergers experienced by the three most massive galaxies in the cluster as a function of redshift.

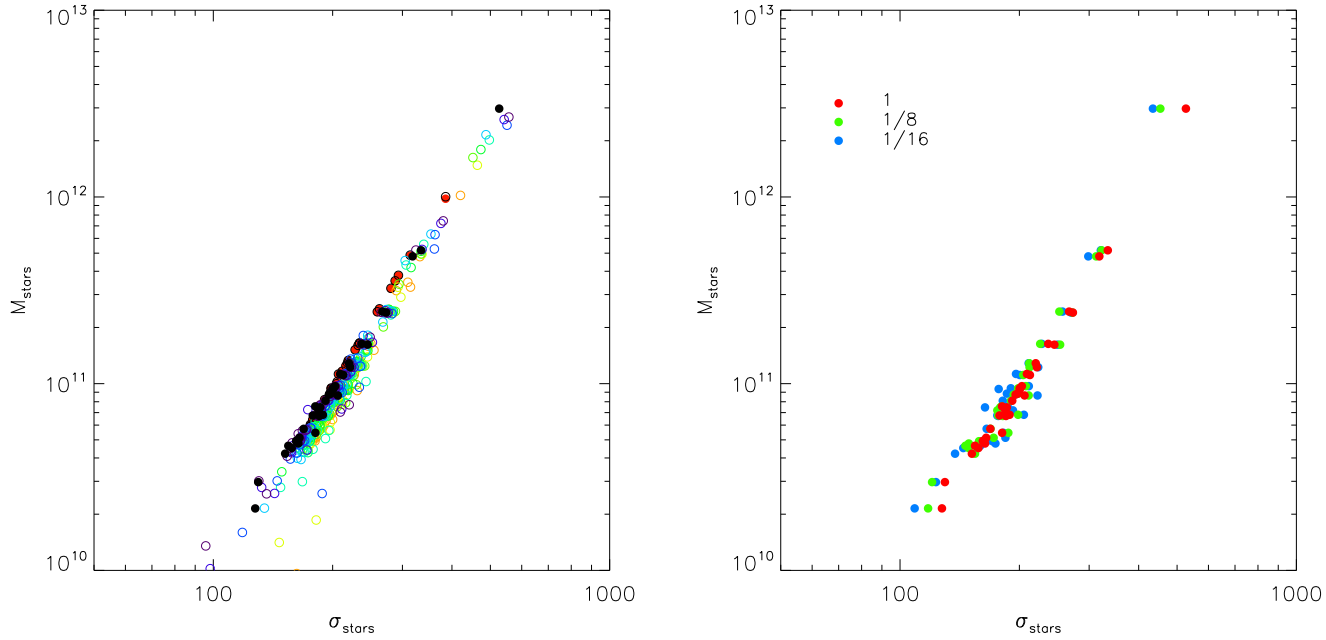


FIG. 4.— Left panel: stellar mass as a function of the flux-weighted line-of-sight stellar velocity dispersion within the half-light radii. The meaning of symbols is the same as in Figure 1. Right panel: flux-weighted line-of-sight stellar velocity dispersion computed for three different apertures (half-light radius, 1/8 and 1/16 of that radius) as a function of the stellar mass at $z = 0$.

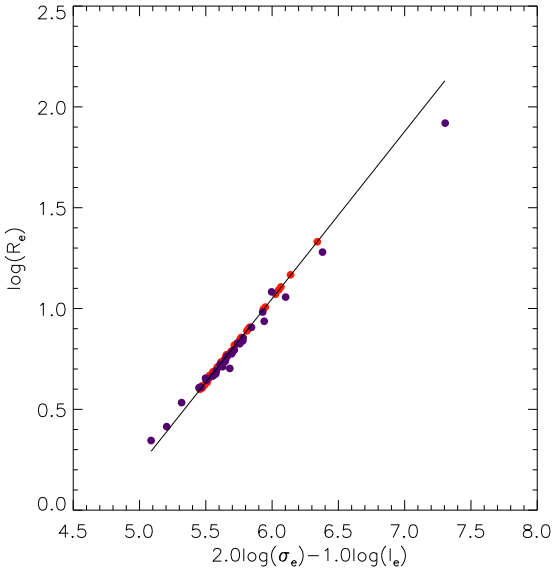


FIG. 5.— Fundamental "plane" for the galaxy model at $z = 3$ (red) and $z = 0$ (violet). R_e and σ_e are the half-light radius and the velocity dispersion defined as in Figure 4. The intensity is defined as $I_e = m_{\rm star}/(\pi R_e^2)$.

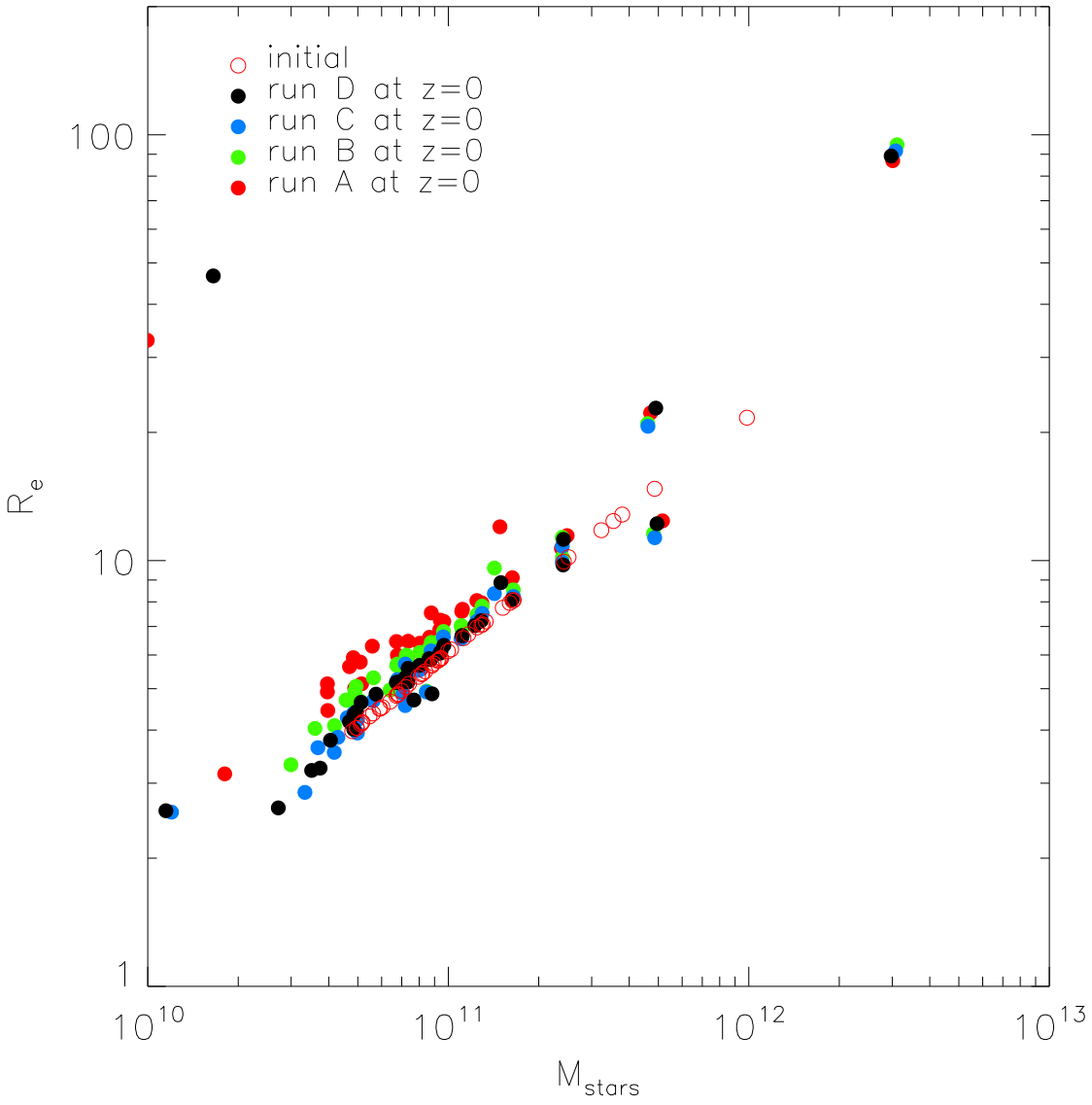


FIG. 6.— Convergence study for the relation between half-light radius and stellar mass, $R_e - M_\star$, for four different runs of increasing numerical resolution (from run A to Run D; see text for details). All filled circles correspond to the galaxies at $z = 0$. Open red circles are for the initial galaxy models at $z = 3$. All runs were carried out for uncontracted galaxy models.

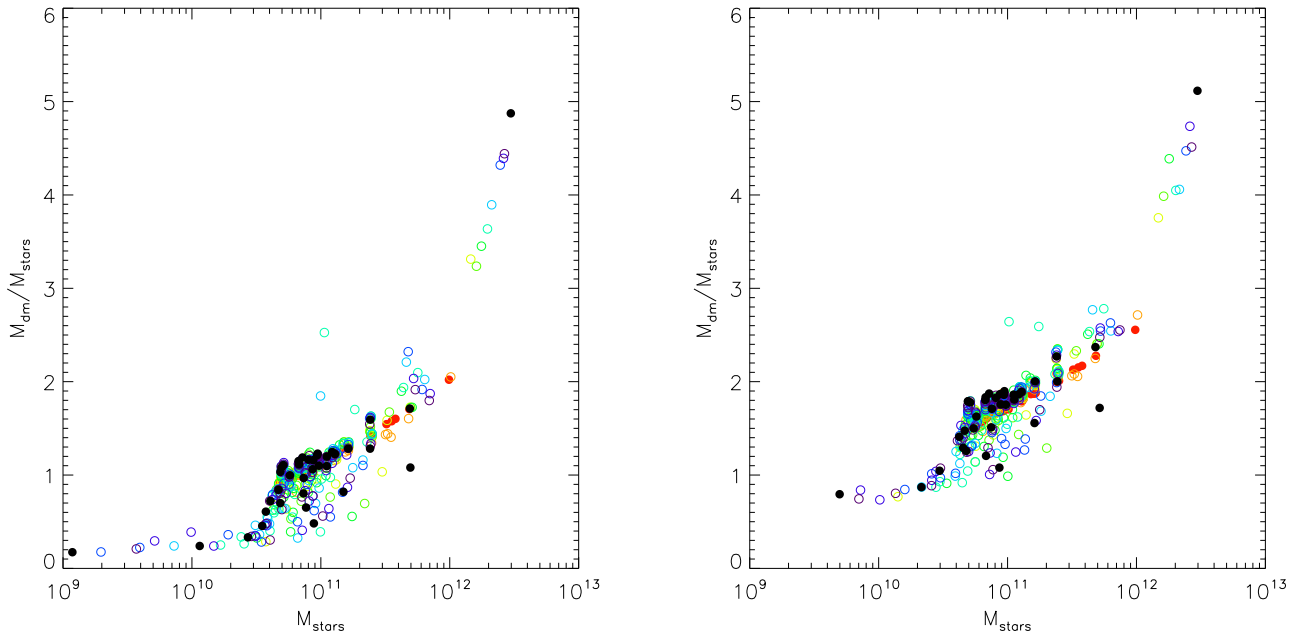


FIG. 7.— Dark matter to stellar mass ratios vs. stellar mass. The meaning of the symbols is the same as in Figure 1. The left panel shows results for uncontracted galaxy models, while the panel on the right gives results for adiabatically compressed initial galaxy models.